

# Cosmological perturbations in the DGP braneworld: numeric solution

Antonio Cardoso,<sup>1,\*</sup> Kazuya Koyama,<sup>1,†</sup> Sanjeev S. Seahra,<sup>1,2,‡</sup> and Fabio P. Silva<sup>1,§</sup>

<sup>1</sup>*Institute of Cosmology & Gravitation, University of Portsmouth, Portsmouth PO1 2EG, UK*

<sup>2</sup>*Department of Mathematics & Statistics, University of New Brunswick*

*Fredericton, New Brunswick, Canada E3B 5A3*

(Dated: December 9, 2007)

We solve for the behaviour of cosmological perturbations in the Dvali-Gabadadze-Porrati (DGP) braneworld model using a new numerical method. Unlike some other approaches in the literature, our method uses no approximations other than linear theory and is valid on large scales. We examine the behaviour of late-universe density perturbations for both the self-accelerating and normal branches of DGP cosmology. Our numerical results can form the basis of a detailed comparison between the DGP model and cosmological observations.

## I. INTRODUCTION

In the braneworld paradigm our universe is a lower-dimensional object embedded in a higher-dimensional bulk spacetime. Standard Model fields are assumed to be confined to the brane while gravity is allowed to propagate in the bulk. The Dvali-Gabadadze-Porrati (DGP) [1, 2] model postulates that we live in a 4-dimensional hypersurface in a 5-dimensional Minkowski bulk. General Relativity (GR) is recovered at small scales (smaller than the crossover scale  $r_c$ ) due to the inclusion of an induced gravity term in the action.

It was quickly realized that this model has two distinct classes of cosmological solutions [3]. One of them exhibits accelerated expansion at late times without the need to include any exotic cosmological fluids, such as dark energy, or any brane tension that acts as an effective 4-dimensional cosmological constant. Hence, this branch of solutions is called “self-accelerating”. Several attempts to confront the self-accelerating universe with observations have been made [4, 5, 6] (also see [7, review] and references therein). To explain the observed acceleration we require  $r_c \sim H_0^{-1}$ , where  $H_0$  is the current value of the Hubble parameter. It is expected that structure formation will help to distinguish the self-accelerating DGP universe from dark energy models based on 4-dimensional GR. This is because the growth of cosmological perturbations is very sensitive to the existence of an extra dimension. A full 5-dimensional treatment is required to model these perturbations, which is why obtaining observational predictions for the behaviour of fluctuations in the DGP model is technically challenging.

Several authors have considered the problem of the dynamics of perturbations in the DGP model, but they have all relied on some sort of approximation or simplifying *ansatz*. Two examples of this are the quasi-static (QS) approximation developed by Koyama and Maartens [8]

and the dynamical scaling (DS) *ansatz* proposed by Sawicki et al. [9]. The former approximation scheme solves the perturbative equations of motion by focussing on the extreme subhorizon regime. In contrast the DS method, which assumes that perturbations evolve as power laws of the scale factor with time-varying power law indices, is supposed to be valid on all scales. It has been shown that the DS solution approaches the QS solution for subhorizon perturbations.

In this paper we present a complete numerical analysis of the evolution of scalar perturbations in the DGP model. Mathematically, the problem involves the solution of a partial differential equation in the bulk coupled to an ordinary differential equation on the brane. A numerical method for dealing with such systems has previously been developed for cosmological perturbations in the Randall-Sundrum (RS) model [10, 11]. However, the DGP problem is more complicated than the RS case due to a non-local boundary condition on the bulk field. Hence, the algorithm used in this paper represents a significant generalization of the one used in Refs. [10, 11].

Unfortunately, some theoretical issues cast doubt on the validity of the self-accelerating DGP solutions. Specifically, the existence of a perturbative ghost perhaps suggests that this solution cannot describe our Universe [12, 13], though there has been a debate on the physical implication of the ghost mode (see [14, review] and references therein). However, as alluded to above there is another “normal” branch of solutions in the DGP model. We cannot explain the late time accelerated expansion of the Universe using the normal branch without including an effective cosmological constant induced by the brane tension  $\sigma$ . However, by allowing a non-zero  $\sigma$ , normal branch solutions can mimic dark energy models with the equation of state  $w$  smaller than  $-1$  [15, 16]. Cosmological constraints on the background dynamics of these models have been studied [17, 18]. Unlike 4-dimensional models that realize  $w < -1$  by the introduction of a phantom field, the normal branch of DGP cosmology is ghost-free [19]. This unique feature is what motivates us to numerically study the perturbations of the normal branch of DGP cosmology in the penultimate section of this paper. During the preparation of this manuscript,

\*Electronic address: antonio.cardoso.AT.port.ac.uk

†Electronic address: kazuya.koyama.AT.port.ac.uk

‡Electronic address: sanjeev.seahra.AT.port.ac.uk

§Electronic address: fabio.silva.AT.port.ac.uk

we learned that the behaviour of perturbations in the normal branch has been independently obtained by Song [20] using the DS method.

The structure of the paper is as follows: The background cosmology of the DGP model is discussed in §II. In §III, we express the equations of motion for scalar and tensor perturbations of the DGP model in the dimensionless canonical form introduced in §III A. The numerical method used to solve these canonical equations of motion is developed in §IV. Our algorithm is tested in §V, where we numerically recover analytic results for the behaviour of tensor perturbations in matter-free DGP models. In §VI and §VII, we solve the scalar perturbations problem in the self-accelerating and normal branches, respectively. Finally, §VIII is reserved for our conclusions.

## II. BACKGROUND SOLUTION

### A. Field equations and junction conditions

We consider a 5-dimensional manifold  $\mathcal{M}$  with metric  $g_{ab}$ , and covered by coordinates  $\{X^a\}_{a=0}^4$ . The manifold has a 4-dimensional brane boundary  $\partial\mathcal{M}_b$  with intrinsic metric  $\gamma_{\alpha\beta}$ , and covered by coordinates  $\{x^\alpha\}_{\alpha=0}^3$ . The action of the model is

$$S = \frac{1}{2\kappa_5^2} \int_{\mathcal{M}} d^5X \sqrt{-g} R^{(5)} + \frac{1}{2\kappa_4^2} \int_{\partial\mathcal{M}_b} d^4x \sqrt{-\gamma} R^{(4)} + \int_{\partial\mathcal{M}_b} d^4x \sqrt{-\gamma} (\mathcal{L}_m - \sigma). \quad (1)$$

Here,  $\sigma$  is the brane tension and  $\mathcal{L}_m$  is the matter Lagrangian. We impose the  $\mathbb{Z}_2$  symmetry that the bulk is mirror symmetric about the brane.<sup>1</sup> The field equations satisfied in  $\mathcal{M}$  are simply

$$R_{ab}^{(5)} = 0. \quad (2)$$

We write the brane normal pointing *into*  $\mathcal{M}$  as  $n^a$ . We find that the brane's extrinsic curvature,

$$K_{\alpha\beta} = e_\alpha^a e_\beta^b \nabla_a n_b, \quad e_\alpha^a = \frac{\partial X^a}{\partial x^\alpha}, \quad (3)$$

must satisfy

$$K_{\alpha\beta} - K\gamma_{\alpha\beta} - r_c G_{\alpha\beta}^{(4)} = -\frac{1}{2}\kappa_5^2 (T_{\alpha\beta} - \sigma g_{\alpha\beta}), \quad (4)$$

where we have defined the cross-over distance  $r_c$  by

$$r_c = \frac{\kappa_5^2}{2\kappa_4^2}. \quad (5)$$

We assume that the stress-energy tensor of the brane matter,

$$T_{\alpha\beta} = -\frac{2}{\sqrt{-\gamma}} \frac{\delta(\sqrt{-\gamma}\mathcal{L}_m)}{\delta\gamma^{\alpha\beta}} = (\rho + p)u_\alpha u_\beta + pg_{\alpha\beta}, \quad (6)$$

is of the perfect fluid form. Note that as in GR, the stress energy tensor is conserved,  $\nabla^\alpha T_{\alpha\beta} = 0$ . Using the Gauss-Codazzi equations, it is possible to re-write the junction conditions (4) as the effective Einstein equations

$$G_{\mu\nu}^{(4)} = (2\kappa_4^2 r_c)^2 \Pi_{\mu\nu} - \mathcal{E}_{\mu\nu}, \quad (7)$$

where

$$\Pi_{\mu\nu} = -\frac{1}{4}\tilde{T}_{\mu\alpha}\tilde{T}_\nu^\alpha + \frac{1}{12}\tilde{T}\tilde{T}_{\mu\nu} + \frac{1}{24}(3\tilde{T}_{\alpha\beta}\tilde{T}^{\alpha\beta} - \tilde{T}^2)g_{\mu\nu}, \\ \tilde{T}_{\mu\nu} = T_{\mu\nu} - \sigma g_{\alpha\beta} - \kappa_4^{-2}G_{\mu\nu}^{(4)}, \quad (8)$$

and  $\mathcal{E}_{\mu\nu}$  is the trace-free projection of the 5-dimensional Weyl tensor.

An important tool that is often used to analyze braneworld models is the ‘‘Gaussian-normal’’ coordinates. These are constructed by looking at the spatial geodesics that extend perpendicularly from  $\partial\mathcal{M}_b$  into  $\mathcal{M}$ . Gaussian-normal coordinates are then given by  $(x^\alpha, y)$ , where  $y$  is the affine parameter along these geodesics and  $x^\alpha$  are 4-dimensional coordinates on the family of hypersurfaces tangent to the brane. Without loss of generality, we can set the brane to be at  $y = 0$ . Most importantly, the derivative of any bulk scalar quantity with respect to  $y$  on the brane corresponds to the normal derivative:

$$(\partial_y \psi)_b = \left. \frac{\partial \psi}{\partial y} \right|_{y=0} = n^a \partial_a \psi. \quad (9)$$

Below,  $(\partial_y \dots)_b$  will always be understood to be the normal derivative of some quantity evaluated at the brane.

### B. Bulk geometry and brane trajectory

One solution of the above field equations makes use of the following 5-dimensional flat metric with  $R_{abcd} = 0$ :

$$ds^2 = g_{ab} dX^a dX^b = -r_c^2 du dv + v^2 d\mathbf{x}^2. \quad (10)$$

Here,  $u$  and  $v$  are dimensionless null coordinates. The brane is defined parametrically by  $(u, v) = (u_b(t), v_b(t))$ , where

$$v_b(t) = a(t), \quad u_b(t) = \frac{1}{r_c^2} \int_0^t \frac{dx}{\dot{a}(x)}. \quad (11)$$

Here,  $a(t)$  is the scale factor of the brane universe, normalized to unity today, and  $t$  is the proper time along the brane. The latter implies that the following induced line element on the brane is of the FRW form:

$$ds_b^2 = \gamma_{\alpha\beta} dx^\alpha dx^\beta = -dt^2 + a^2(t) d\mathbf{x}^2. \quad (12)$$

<sup>1</sup> Technically,  $\mathcal{M}$  refers to one half of the total bulk spacetime.

We have selected the  $u$  coordinate such that  $u_b(0) = 0$  and the brane moves in the direction of increasing  $u$  and  $v$ . The 5-velocity of the brane  $u^a$  and brane normal  $n^a$  are given by

$$\partial_t = u^a \partial_a = \frac{dx^a}{dt} \frac{\partial}{\partial x^a} = \frac{1}{r_c^2 \dot{a}} \partial_u + \dot{a} \partial_v, \quad (13a)$$

$$\partial_y = n^a \partial_a = \epsilon \left[ -\frac{1}{r_c^2 \dot{a}} \partial_u + \dot{a} \partial_v \right]. \quad (13b)$$

These satisfy

$$u^a u_a = -1, \quad u^a n_a = 0, \quad n^a n_a = 1. \quad (14)$$

The  $\epsilon = \pm 1$  parameter in the definition of the brane normal (13b) reflects the fact that when we impose the  $\mathbb{Z}_2$  symmetry across the brane, we have two choices for the half of the bulk manifold  $\mathcal{M}$  we discard.

The junction conditions (4) can be used to determine the brane dynamics, which are governed by

$$H = \frac{\dot{a}}{a} = \frac{1}{2r_c} \left[ \epsilon + \sqrt{1 + \frac{4}{3} \kappa_4^2 r_c^2 (\rho + \sigma)} \right], \quad (15a)$$

$$\frac{d\rho}{dt} = -3(1+w)\rho H, \quad (15b)$$

$$\frac{dH}{dt} = -\frac{r_c \kappa_4^2 (1+w)\rho H}{\sqrt{1 + \frac{4}{3} r_c^2 \kappa_4^2 (\rho + \sigma)}}. \quad (15c)$$

Note that when  $\epsilon = +1$ , we have that  $Hr_c \approx 1$  when the density of brane matter is small  $|\rho + \sigma| \ll \kappa_4^{-2} r_c^{-2}$ . This implies a late-time accelerating universe, which is why the  $\epsilon = +1$  case is called the self-accelerating branch and the  $\epsilon = -1$  case is called the normal branch.

### III. MASTER EQUATIONS GOVERNING PERTURBATIONS

#### A. Dimensionless coordinates and canonical wave equations

In this paper, we will consider the perturbations of the DGP model governed by a field  $\psi$  defined on the bulk spacetime  $\mathcal{M}$  coupled to a dynamical field  $\Delta$  residing on the brane  $\partial\mathcal{M}_b$ . It is useful to decompose these fields into Fourier modes as follows:

$$\psi(u, v, \mathbf{x}) = \int \frac{d^3 \mathbf{k}}{(2\pi)^{3/2}} \psi_{\mathbf{k}}(u, v) e^{i\mathbf{k} \cdot \mathbf{x}}, \quad (16a)$$

$$\Delta(t, \mathbf{x}) = \int \frac{d^3 \mathbf{k}}{(2\pi)^{3/2}} \Delta_{\mathbf{k}}(t) e^{i\mathbf{k} \cdot \mathbf{x}}. \quad (16b)$$

As usual for linear theory, the individual  $\mathbf{k}$  modes are decoupled from one another. In what follows, we will omit the  $\mathbf{k}$  subscript from  $\psi_{\mathbf{k}}$  and  $\Delta_{\mathbf{k}}$ . That is,  $\psi$  and  $\Delta$  refer to the Fourier amplitudes of modes with wavevector  $\mathbf{k}$ . We will also assume that a normalization has been

selected such that the Fourier amplitudes are dimensionless.

For a given mode, we define the “\*” epoch as the moment when a given mode crosses the Hubble horizon:

$$k = H_* a_*, \quad k^2 = \mathbf{k} \cdot \mathbf{k}. \quad (17)$$

Then, we can define a set of normalized variables (decorated with hats):

$$\begin{aligned} \hat{H} &= Hr_c, & \hat{k} &= kr_c/a_*, & \hat{\rho} &= \kappa_4^2 r_c^2 \rho, \\ \hat{\sigma} &= \kappa_4^2 r_c^2 \sigma, & \hat{t} &= t/r_c, & \hat{y} &= y/r_c, \\ \hat{a} &= a/a_*, & \hat{u} &= a_* u, & \hat{v} &= v/a_*. \end{aligned} \quad (18)$$

Explicitly, we have

$$\hat{H} = \frac{1}{2} \left[ \epsilon + \sqrt{1 + \frac{4}{3} (\hat{\rho} + \hat{\sigma})} \right], \quad (19a)$$

$$\hat{k} = \frac{1}{2} \left[ \epsilon + \sqrt{1 + \frac{4}{3} (\hat{\rho}_* + \hat{\sigma})} \right] = \hat{H}_*. \quad (19b)$$

It is also useful to define the 2-dimensional Cartesian coordinates

$$x^0 = \tau = \frac{\hat{v} + \hat{u}}{2}, \quad x^1 = z = \frac{\hat{v} - \hat{u}}{2}. \quad (20)$$

In terms of these coordinates, the dimensionless tangential  $\hat{\partial}_t = U^A \partial_A$  and normal  $\hat{\partial}_y = N^A \partial_A$  derivatives to the brane are

$$\hat{\partial}_t = \frac{1}{2} \left[ \left( \hat{H} \hat{a} + \frac{1}{\hat{H} \hat{a}} \right) \frac{\partial}{\partial \tau} + \left( \hat{H} \hat{a} - \frac{1}{\hat{H} \hat{a}} \right) \frac{\partial}{\partial z} \right], \quad (21a)$$

$$\hat{\partial}_y = \frac{\epsilon}{2} \left[ \left( \hat{H} \hat{a} - \frac{1}{\hat{H} \hat{a}} \right) \frac{\partial}{\partial \tau} + \left( \hat{H} \hat{a} + \frac{1}{\hat{H} \hat{a}} \right) \frac{\partial}{\partial z} \right], \quad (21b)$$

where

$$-1 = U_A U^A, \quad 1 = N_A N^A, \quad 0 = U_A N^A, \quad (22)$$

and capital roman indices  $A, B = 0, 1$  are raised and lowered with the flat 2-metric  $\eta_{AB} = \text{diag}(-1, 1)$ .

The brane trajectory in the  $(\tau, z)$  plane is given by the solution of

$$\frac{d\hat{a}}{d\hat{t}} = \hat{H} \hat{a}, \quad (23a)$$

$$\frac{d\tau_b}{d\hat{t}} = \frac{1}{2} \left( \hat{H} \hat{a} + \frac{1}{\hat{H} \hat{a}} \right), \quad (23b)$$

$$\frac{dz_b}{d\hat{t}} = \frac{1}{2} \left( \hat{H} \hat{a} - \frac{1}{\hat{H} \hat{a}} \right), \quad (23c)$$

subject to the initial conditions

$$\hat{a}(0) = \hat{a}_i, \quad \tau_b(0) = \frac{1}{2} \hat{a}_i, \quad z_b(0) = \frac{1}{2} \hat{a}_i. \quad (24)$$

If  $\epsilon = +1$ , the normal points in the direction of increasing  $z$  and the “bulk” corresponds to the the portion of

the  $(\tau, z)$  plane to the right of the brane; if  $\epsilon = -1$  the opposite is true.

We will find below that the equations governing the bulk  $\psi = \psi(\tau, z)$  and brane field  $\Delta = \Delta(\hat{t})$  are of the form:

$$0 = (\partial_\tau^2 - \partial_z^2 + V)\psi, \quad (25a)$$

$$(\partial_{\hat{y}}\psi)_b = \lambda_1\Delta + \lambda_2\Xi + \lambda_3\psi_b + \lambda_4\psi'_b + \lambda_5\psi''_b, \quad (25b)$$

$$\Xi' = \lambda_6\Delta + \lambda_7\Xi + \lambda_8\psi_b + \lambda_9\psi'_b + \lambda_{10}\psi''_b, \quad (25c)$$

$$\Delta' = \Xi, \quad (25d)$$

where we have introduced the auxiliary field  $\Xi$ , which corresponds to the time derivative of  $\Delta$ . In (25), a prime ' denotes the derivative with respect to the dimensionless proper time  $d/d\hat{t}$  and  $\psi_b = \psi_b(\hat{t}) = \psi(\tau_b(\hat{t}), z_b(\hat{t}))$  is the value of the bulk field on the brane. Also,  $V = V(\tau, \hat{z})$  is the bulk potential and the coefficients  $\lambda_n = \lambda_n(\hat{a})$  are functions of the brane scale factor. All quantities appearing in (25) are dimensionless. We refer to (25) as the canonical form of the perturbative equations of motion.

## B. Density perturbations in the late universe

In this subsection we describe the formulae governing scalar perturbations in the late-time matter dominated universe. We take the matter content of the brane to be a dust fluid  $w = 0$  (i.e., cold dark matter):

$$\rho \propto a^{-3}. \quad (26)$$

In the 5-dimensional longitudinal gauge, scalar-type perturbations<sup>2</sup> of the bulk geometry (10) can be written as

$$ds^2 = -r_c^2(du dv + F_{uu}du^2 + 2F_{uv}du dv + F_{vv}dv^2) + r_c(f_{ui}du + f_{vi}dv)dx^i + v^2(1 + 2\mathcal{R})\delta_{ij}dx^i dx^j. \quad (27)$$

It can be shown that the dynamics of all of the perturbative quantities in this expression can be derived from a single scalar bulk degree of freedom [21]. After Fourier decomposition, we find that the mode amplitude  $\Omega = \Omega(u, v)$  of this master field obeys

$$0 = \frac{\partial^2 \Omega}{\partial u \partial v} - \frac{3}{2v} \frac{\partial \Omega}{\partial u} + \frac{k^2 r_c^2}{4v^2} \Omega. \quad (28)$$

We parameterize the fluctuations of the brane geometry by the two metric potentials  $\Phi$  and  $\Psi$ :

$$ds_b^2 = -(1 + 2\Psi)dt^2 + a^2(1 + 2\Phi)\delta_{ij}dx^i dx^j. \quad (29)$$

Finally, we write the perturbation of the brane fluid stress energy tensor as

$$\delta T^0_0 = -\delta\rho, \quad \delta T^0_i = a \partial_i \delta q, \quad \delta T^i_j = \delta p \delta^i_j. \quad (30)$$

One can construct the comoving density perturbation from these quantities as follows:

$$\rho\Delta = \delta\rho - 3Ha \delta q. \quad (31)$$

Both  $\Delta$  and  $\Omega$  are gauge invariant quantities under a coordinate transformation on the brane and in the bulk. Note that  $\Delta$  is the density contrast of the cold dark matter only, not the the total density contrast.

As shown in [22] and demonstrated in Appendix A, one can use the effective Einstein equations on the brane and the detailed relationship between  $\Omega$  and the metric perturbations to find the following boundary condition for  $\Omega$ :

$$(\partial_y \Omega)_b = -\frac{\epsilon\gamma_1}{2H}\ddot{\Omega}_b + \frac{9\epsilon\gamma_3}{4}\dot{\Omega}_b - \frac{3(\epsilon\gamma_3 k^2 + \gamma_4 H^2 a^2)}{4Ha^2}\Omega_b + \frac{3\epsilon r_c \kappa_4^2 \rho a^3 \gamma_4}{2k^2}\Delta; \quad (32)$$

the following equation of motion for  $\Delta$ :

$$\ddot{\Delta} + 2H\dot{\Delta} - \frac{1}{2}\kappa_4^2 \rho \gamma_2 \Delta = -\frac{\epsilon\gamma_4 k^4}{4a^5}\Omega_b; \quad (33)$$

and the following expressions for  $\Phi$  and  $\Psi$ :

$$\begin{aligned} \Phi &= +\frac{\kappa_4^2 \rho a^2 \gamma_1}{2k^2}\Delta + \frac{\epsilon\gamma_1}{4ar_c}\dot{\Omega}_b - \frac{\epsilon(k^2 + 3H^2 a^2)\gamma_1}{12Hr_c a^3}\Omega_b, \\ \Psi &= -\frac{\kappa_4^2 \rho a^2 \gamma_2}{2k^2}\Delta + \frac{\epsilon\gamma_1}{4Hr_c a}\dot{\Omega}_b - \frac{3\epsilon H \gamma_4}{4a}\dot{\Omega}_b + \\ &\quad \frac{\epsilon(k^2 r_c \gamma_4 + H a^2 \gamma_2)}{4r_c a^3}\Omega_b, \end{aligned} \quad (34)$$

where  $\Omega_b = \Omega_b(t) = \Omega(u_b(t), v_b(t))$ . In these expressions, the dimensionless  $\gamma$ -factors are:

$$\gamma_1 = \frac{2\epsilon H r_c}{2\epsilon H r_c - 1}, \quad (35a)$$

$$\gamma_2 = \frac{2\epsilon r_c(\dot{H} - H^2 + 2\epsilon H^3 r_c)}{H(2\epsilon H r_c - 1)^2}, \quad (35b)$$

$$\gamma_3 = \frac{4\epsilon r_c(2\epsilon r_c \dot{H} - 3H + 6\epsilon H^2 r_c)}{9(2\epsilon H r_c - 1)^2}, \quad (35c)$$

$$\gamma_4 = \frac{4\epsilon(\epsilon r_c \dot{H} - H + 2\epsilon H^2 r_c)}{3H(2\epsilon H r_c - 1)^2}. \quad (35d)$$

From these formulae, it follows that the bulk field  $\Omega$  has dimensions of (length)<sup>2</sup>. The bulk wave equation (28), boundary condition (32) and (33) are the equations we must solve. Once we know  $\Delta$  and  $\Omega$  the metric perturbations  $\Phi$  and  $\Psi$  can be obtained by differentiation. Another quantity of interest is the curvature perturbation in uniform density slices, which is given by

$$\zeta = \Phi + \frac{Ha}{\rho}\delta q + \frac{1}{3}\Delta, \quad (36)$$

<sup>2</sup> That is, perturbations that can be derived from scalar potentials defined on the 3-dimension spatial sections.

coefficient	scalar case (matter domination)	tensor case (pure tension brane)
$\lambda_1$	$\frac{3}{2}\epsilon\hat{\rho}\hat{a}^{3/2}\hat{k}^{-2}\gamma_4$	0
$\lambda_2$	0	0
$\lambda_3$	$-\frac{3}{4}\epsilon\hat{H}^{-1}\hat{H}'\gamma_1 - \frac{3}{8}\epsilon\hat{H}(4 + 3\gamma_1 - 9\gamma_3 + 2\epsilon\gamma_4) - \frac{3}{4}\epsilon\hat{k}^2\hat{H}^{-1}\hat{a}^{-2}\gamma_3$	$\hat{k}^2\hat{a}^{-2} + \frac{3}{4}\hat{H}(2\epsilon - \hat{H})$
$\lambda_4$	$\frac{3}{4}\epsilon(3\gamma_3 - 2\gamma_2)$	0
$\lambda_5$	$-\frac{1}{2}\epsilon\hat{H}^{-1}\gamma_1$	1
$\lambda_6$	$\frac{1}{2}\hat{\rho}\gamma_2$	0
$\lambda_7$	$-2\hat{H}$	0
$\lambda_8$	$-\frac{1}{4}\epsilon\hat{k}^4\hat{a}^{-7/2}\gamma_4$	0
$\lambda_9$	0	0
$\lambda_{10}$	0	0
$\lambda_{11} = \lambda'_5$	$\frac{1}{2}\epsilon\hat{H}^{-2}\hat{H}'\gamma_1$	0
$\lambda_{12} = \lambda'_{10}$	0	0

TABLE I: Dimensionless coefficients appearing in the canonical wave equations (25) for the case of scalar perturbations in the late universe and tensor perturbation of a pure tension brane. Even though the  $\lambda_{11}$  and  $\lambda_{12}$  coefficients do not appear in (25), they are crucial for the numeric scheme developed in §IV. We make use of the  $\gamma$ -factors defined in Eq. (35) and the following notation:  $\hat{H}' = d\hat{H}/d\hat{t} = -(1+w)\hat{\rho}(1 + \frac{4}{3}\hat{\mu})^{-1/2}$ ,  $\hat{\mu} = \hat{\rho} + \hat{\sigma}$ , and  $\hat{\rho} = \hat{\rho}_*\hat{a}^{-3}$ .

assuming matter domination. This can be explicitly represented in terms of  $\Delta$  and  $\Omega_b$ :

$$\zeta = \left( \frac{1}{3} + \frac{\kappa_4^2 \rho a^2 \gamma_1}{2k^2} \right) \Delta + \frac{Ha^2}{k^2} \dot{\Delta} - \frac{\epsilon \gamma_1 k^2}{12Hr_c a^3} \Omega_b. \quad (37)$$

This quantity is interesting because it is expected to be conserved on superhorizon scales for any metric theory of gravity [23], including the DGP model. Hence, an explicit verification that  $\zeta$  is constant when  $k \ll Ha$  provides a useful consistency check of our numerical code.

We can define a dimensionless canonical bulk field  $\psi$  by

$$\psi = \frac{a_*^{1/2}}{v^{3/2} r_c^2} \Omega. \quad (38)$$

Substitution of this into (28) confirms that  $\psi$  satisfies the canonical bulk wave equation (25a) with potential

$$V(\tau, z) = \frac{\hat{k}^2}{(\tau + z)^2}. \quad (39)$$

We can then replace  $\Omega$  with  $\psi$  in (32) and (33) and make use of (18) to obtain the canonical boundary condition (25b) and  $\Delta$  equation of motion (25c). The explicit expressions for the dimensionless  $\lambda_n$  coefficients are given in Table I. Finally, it is useful to define a dimensionless version of  $\Omega$  as follows:

$$\hat{\Omega} = \hat{v}^{3/2} \psi = a_*^{-1} r_c^{-2} \Omega. \quad (40)$$

Generally speaking, it is more useful to work with  $\hat{\Omega}$  than  $\Omega$  for numeric computations, and later on we will present plots of  $\hat{\Omega}$  instead of  $\Omega$ .

### C. Tensor perturbations

For tensor perturbations, we restrict ourselves to cases where there is no ordinary matter on the brane,

$$\hat{\rho} = 0, \quad \hat{\sigma} = 3Hr_c(Hr_c - \epsilon). \quad (41)$$

Tensor type perturbations of the bulk geometry are described by perturbations of the form:

$$ds^2 = -r_c^2 du dv + v^2 (\delta_{ij} + E_{ij}) dx^i dx^j, \quad (42)$$

where the 3-tensor  $E_{ij}$  is given by

$$E_{ij} = \sum_{A=\oplus, \otimes} \int \frac{d^3k}{(2\pi)^{3/2}} E_{\mathbf{k}}^A(u, v) e^{i\mathbf{k}\cdot\mathbf{x}} e_{ij}^A(\mathbf{k}). \quad (43)$$

Here,  $e_{ij}^A$  is a constant polarization tensor satisfying

$$\partial_a e_{ij}^A(\mathbf{k}) = \delta^{ij} e_{ij}^A(\mathbf{k}) = k^i e_{ij}^A(\mathbf{k}) = 0. \quad (44)$$

For brevity, we omit the  $\mathbf{k}$  subscript and  $A$  superscript on the mode amplitude  $E_{\mathbf{k}}^A(u, v)$  below. Perturbations of the bulk Einstein equations yield

$$\delta R_{ab}^{(5)} = 0 \quad \Rightarrow \quad 0 = \frac{\partial^2 E}{\partial u \partial v} + \frac{3}{2v} \frac{\partial E}{\partial u} + \frac{k^2 r_c^2}{4v^2} E. \quad (45)$$

Note that this is equivalent to  $\nabla^a \nabla_a (E e^{i\mathbf{k}\cdot\mathbf{x}}) = 0$ . Perturbation of the junction conditions yields that

$$(\partial_y E)_b = r_c \left( \ddot{E}_b + 3H\dot{E}_b + \frac{k^2}{a^2} E_b \right). \quad (46)$$

To bring this into the canonical form we introduce the new bulk variable

$$\psi = \frac{v^{3/2}}{a_*} E, \quad (47)$$

which satisfies the canonical bulk wave equation with potential

$$V(\tau, z) = \frac{\hat{k}^2}{(\tau + z)^2}. \quad (48)$$

Substitution of (47) into the boundary condition (46) yields the other canonical coefficients  $\lambda_n$  in (25), which are listed in Table I. Note that since there is no brane field  $\Delta$  in this case, we set  $\lambda_n = 0$  for  $n = 1, 2, 6, 7, 8, 9, 10$ .

## IV. NUMERIC METHOD

### A. Computational grid

In this section, we develop a numeric algorithm to solve the system of equations (25) over a finite region  $\Sigma$  of the  $(\tau, z)$  plane. Illustrations of the shape of  $\Sigma$  are given in Fig. 1 for a few different brane trajectories and choices of  $\epsilon$ . The computational domain has three distinct boundaries: the brane  $\partial\Sigma_b$ , a past null hypersurface  $\partial\Sigma_-$ , and a future null hypersurface  $\partial\Sigma_+$ . Note how the computational domain is to the right of  $\partial\Sigma_b$  for the self-accelerating case  $\epsilon = +1$  and to the left for the normal case  $\epsilon = -1$ . The brane size at the beginning of the simulation (where  $\partial\Sigma_b$  and  $\partial\Sigma_-$  intersect, marked  $i$  in the figure) is  $\hat{a}_i$ , while the size at the end (where  $\partial\Sigma_b$  and  $\partial\Sigma_+$  intersect) is  $\hat{a}_f$ .

Our numerical algorithm employs an irregular computational grid as shown in Figs. 1 and 2. To define this grid, we introduce an arbitrary time parametrization along the brane given by the monotonically increasing function  $x = x(\hat{t})$ . The portion of the brane between  $\hat{a} = \hat{a}_i$  and  $\hat{a} = \hat{a}_f$  is subdivided into piecewise linear segments equally spaced in the new  $x$  parameter. That is, the change in  $x$  over a given segment is  $\delta x = h$ , where  $h$  is the overall stepsize parameter of the algorithm. The bulk grid is then completed by drawing null lines emanating from the endpoints of these segments as shown in Fig. 1. As in previous work, the grid involves a number of triangular cells adjacent to the brane and diamond shaped cells in the bulk. The bulk cells will generally not be uniform in size due to our choice of brane partitioning.

Our actual choice of  $x = x(\hat{t})$  is motivated by the desire to obtain a quickly-converging algorithm that samples the expansion history of the brane sufficiently densely. We have experimented with a number of possibilities and have found that  $x(\hat{t}) = \ln \tau_b(\hat{t})$  works best for the self-accelerating branch. On the other hand,  $x(\hat{t}) = \tau_b(\hat{t})$  seems to give good performance for the normal branch. Of course, the choice of  $x$  ultimately does not matter since all possibilities should give the same results in the  $h \rightarrow 0$  limit.

### B. Evolution near the brane

In order to model the evolution of  $\Delta$  and  $\psi$  near the brane, consider the geometry shown in Fig. 2. Roughly speaking, our goal here is to develop an algorithm to calculate the values of the fields at the nodes G and H given the knowledge of their values at (A,D,E,F).

If we integrate the bulk wave equation over the triangular cell EHF, we obtain

$$2\psi_F - \psi_H - \psi_E = \int_{\Delta} d^2x V\psi + \int_E^H d\hat{t} \partial_{\hat{y}}\psi = \int_{\Delta} d^2x V\psi + \int_E^H d\hat{t} (\lambda_1\Delta + \lambda_2\Xi + \lambda_3\psi_b + \lambda_4\psi'_b + \lambda_5\psi''_b). \quad (49)$$

Here, we have used (25b) to substitute for the normal derivative of  $\psi$ . We can also integrate (25c) and (25d) over the brane segment from E to H, we get

$$\begin{aligned} \Xi_H - \Xi_E &= \int_E^H d\hat{t} (\lambda_6\Delta + \lambda_7\Xi + \lambda_8\psi_b + \lambda_9\psi'_b + \lambda_{10}\psi''_b), \\ \Delta_H - \Delta_E &= \int_E^H d\hat{t} \Xi. \end{aligned} \quad (50)$$

We now replace the integrals in the exact expressions (49) and (50) with discrete approximations. First, let us consider the 2-dimensional integral in (49). A simple linear approximation to  $\psi$  inside EHF yields

$$\int_{\Delta} d^2x V\psi = \frac{\delta\hat{t}^2}{12} (V_E\psi_E + V_H\psi_H + V_F\psi_F) + \mathcal{O}(\delta\hat{t}^4). \quad (51)$$

Here,  $\delta\hat{t}$  is the proper time interval between the nodes E and H, which is explicitly

$$\delta\hat{t} = \int_E^H d\hat{t} = \int_E^H dx \Upsilon = \frac{1}{2}h\langle\Upsilon\rangle + \mathcal{O}(h^3). \quad (52)$$

Here, we have introduced the notation

$$\langle X \rangle = X_H + X_E, \quad \|X\| = X_H - X_E, \quad (53)$$

and defined

$$\Upsilon = \frac{d\hat{t}}{dx} = \frac{d\hat{t}}{d\tau_b} \frac{d\tau_b}{dx} = \left[ \frac{1}{2} \left( \frac{\hat{H}\hat{a}}{\hat{H}\hat{a}} + \frac{1}{\hat{H}\hat{a}} \right) \right]^{-1} \frac{d\tau_b}{dx}. \quad (54)$$

The last equality in (52) follows from the trapezoidal approximation for one-dimensional integrals. We use this same approximation for the other line integrals in (49) and (50), after integration by parts to remove the  $\psi''_b$  terms and a change of variables from  $\hat{t}$  to  $x$ . It is useful to simplify the notation by introducing some new coefficients:

$$\begin{aligned} c_1 &= \frac{1}{2}\Upsilon\lambda_1, & c_6 &= \frac{1}{2}\Upsilon\lambda_6, & c_{11} &= \frac{1}{2}\Upsilon. \\ c_2 &= \frac{1}{2}\Upsilon\lambda_2, & c_7 &= \frac{1}{2}\Upsilon\lambda_7, \\ c_3 &= \frac{1}{2}\Upsilon\lambda_3, & c_8 &= \frac{1}{2}\Upsilon\lambda_8, \\ c_4 &= \frac{1}{2}(\lambda_4 - \lambda'_5), & c_9 &= \frac{1}{2}(\lambda_9 - \lambda'_{10}), \\ c_5 &= \Upsilon^{-1}\lambda_5, & c_{10} &= \Upsilon^{-1}\lambda_{10}, \end{aligned} \quad (55)$$

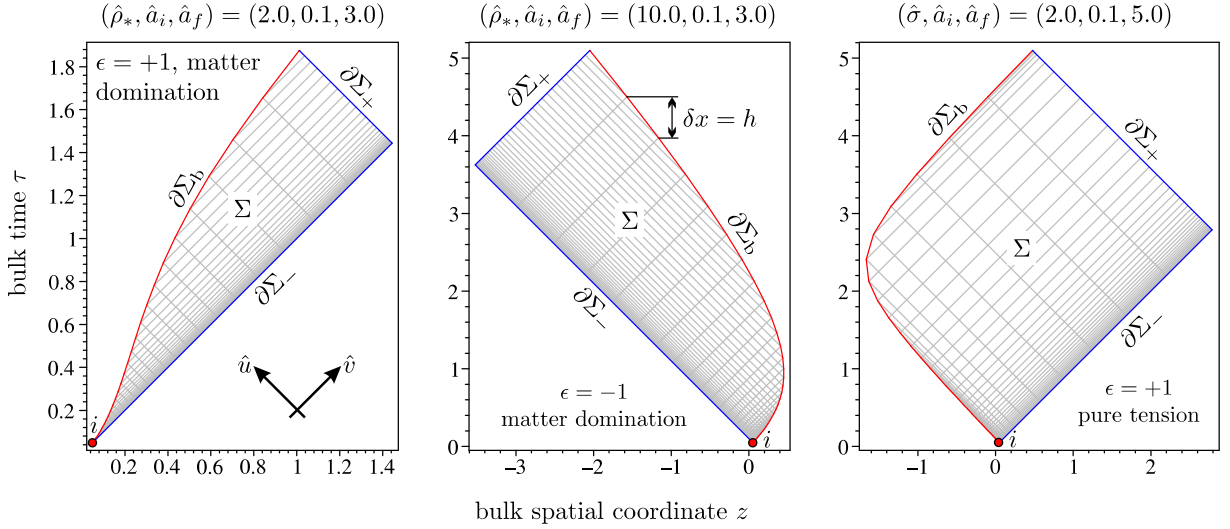


FIG. 1: Typical computational grids used to solve the perturbation equations.

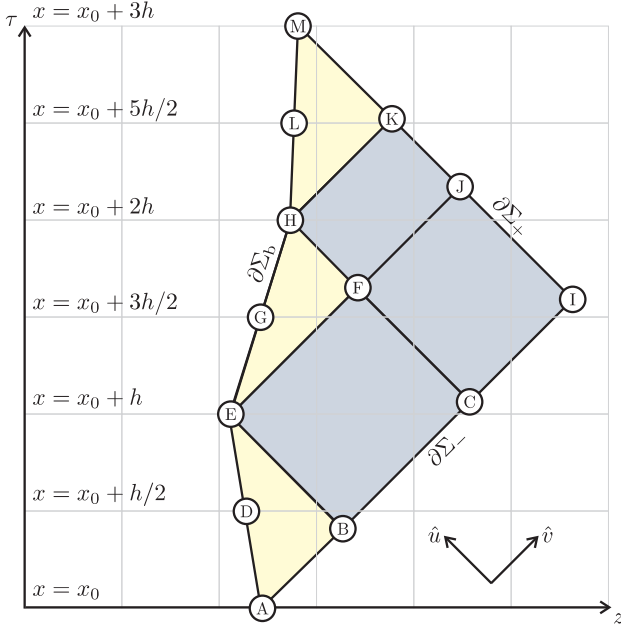


FIG. 2: Grid geometry used to derive evolution formulae in §IV B and §IV C. The principal brane nodes A, E, H and M are separated by a brane time interval  $\delta x = h$ . We have also introduced half-step nodes D, G and L, which are separated from the adjacent principal nodes by  $\delta x = h/2$ . The half-step nodes are needed because of the non-local nature of the boundary condition in the DGP model.

that they are known *exactly*. In terms of these we get

$$2\psi_F - \langle \psi \rangle = h \langle c_1 \Delta + c_2 \Xi + c_3 \psi_b + c_4 \psi_b^\bullet \rangle + \|c_5 \psi_b^\bullet\| + \frac{1}{12} h^2 \langle c_{11} \rangle^2 [\langle V \psi \rangle + V_F \psi_F] + \mathcal{O}(h^3), \quad (56a)$$

$$\|\Xi\| = h \langle c_6 \Delta + c_7 \Xi + c_8 \psi_b + c_9 \psi_b^\bullet \rangle + \|c_{10} \psi_b^\bullet\| + \mathcal{O}(h^3), \quad (56b)$$

$$\|\Delta\| = h \langle c_{11} \Xi \rangle + \mathcal{O}(h^3), \quad (56c)$$

where

$$\psi_b^\bullet = \frac{d\psi_b}{dx} = \frac{d\psi_b}{dt} \frac{dt}{dx} = \Upsilon \psi_b'. \quad (57)$$

We can now make use of the following approximations:

$$\psi_E^\bullet = \frac{12\psi_E - 16\psi_D + 3\psi_A + \psi_H}{6h} + \mathcal{O}(h^3), \quad (58a)$$

$$\psi_H^\bullet = \frac{-36\psi_E + 32\psi_D - 9\psi_A + 13\psi_H}{6h} + \mathcal{O}(h^3), \quad (58b)$$

to eliminate the  $\psi$  derivatives in (56) to order  $h^3$ . Once (58) is substituted into (56), we have a linear system for  $(\psi_H, \Delta_H, \Xi_H)$  in terms of the values of  $\psi$  at the nodes (A, D, E, F), the value of  $\Delta$  and  $\Xi$  at E, and  $h$ . Once this linear system is solved<sup>3</sup> we know the values of all the fields at H (accurate to order  $h^3$ ). Finally, we can use

$$\psi_G = \frac{3}{2}\psi_E - \psi_D + \frac{1}{4}\psi_H + \frac{1}{4}\psi_A + \mathcal{O}(h^4), \quad (59)$$

to get the value of  $\psi$  at G. Note that the values of  $\Delta$  and  $\Xi$  at the nodes D and G have not entered the discussion; it turns out that it is not necessary to keep track of the brane degrees of freedom at non-vertex nodes.

It is worthwhile noting that all of these  $c_i$  coefficients are functions of the brane trajectory only, and we assume

<sup>3</sup> Although this is simple to do, the explicit solution is rather long and we omit it from the current discussion.

### C. Evolution in the bulk

In addition to evolving  $\psi$ ,  $\Delta$  and  $\Xi$  near the brane, we also need to evolve  $\psi$  in the bulk. We can take the diamond CIJF to be a typical bulk cell. By simply integrating the bulk wave equation (25a) over this cell and using the divergence theorem, we obtain

$$2(\psi_F + \psi_I - \psi_J - \psi_C) = \int_{\diamond} d^2x V\psi. \quad (60)$$

Using a bilinear approximation for the integrand yields

$$\begin{aligned} \psi_J = & \psi_F + \psi_I - \psi_C + \frac{1}{16}\delta\hat{u}\delta\hat{v}[V_F\psi_F + \\ & V_C\psi_C + V_I\psi_I + V_J(\psi_F + \psi_I - \psi_C)] + \mathcal{O}(h^4). \end{aligned} \quad (61)$$

Here,  $\delta\hat{u} = \mathcal{O}(h)$  and  $\delta\hat{v} = \mathcal{O}(h)$  are the dimensions of the cell in null coordinates. Hence, given the knowledge of  $\psi$  on the past nodes F, I and C, we can obtain the value at the node J accurate to order  $h^3$ .

### D. Initial data and computational algorithm

Having obtained the formulae that tell us how to evolve the fields across individual cells, we are now in a position to discuss our overall computational strategy. For simplicity, we will describe how the calculation is carried out on the sparse grid shown in Fig. 2, but the method is easily generalized to the denser grids shown in Fig. 1.

For the numeric solution of a conventional hyperbolic problem, it would be sufficient to specify initial data for  $\psi$  on the nodes (A,B,C,I) in addition to  $\Delta_A$  and  $\Xi_A$ . However, due to the nonlocal boundary condition associated with DGP perturbations, we need to also specify  $\psi_D$ ,  $\psi_E$ ,  $\Delta_E$ , and  $\Xi_E$  initially (see [24] for a detailed discussion of wellposedness and initial conditions for DGP perturbations). Once the initial data has been selected, the algorithm proceeds as follows:

1. the diamond evolution formulae (61) is then used to obtain  $\psi$  at the nodes F and J;
2. the triangle evolution algorithm developed in §IV B gives  $\psi_G$ ,  $\psi_H$ ,  $\Delta_H$ , and  $\Xi_H$ ;
3. Eq. (61) is then used to find  $\psi_K$ ; and finally,
4. the triangle algorithm gives the field values at the remaining nodes L and M.

Obviously, if we have a larger grid than the one shown in Fig. 2, steps 2 and 3 need to be iterated a number of times.

For generic grids, the number of diamond cells in the grid will scale as  $1/h^2$  while the number of triangle cells goes like  $1/h$ . Since the errors involved in the diamond and triangle evolution formula are  $\mathcal{O}(h^4)$  and  $\mathcal{O}(h^3)$ , respectively, we obtain a final answer that is quadratically  $\mathcal{O}(h^2)$  convergent.

## V. TENSOR PERTURBATIONS ABOUT A DE SITTER BRANE

It is possible to analytically solve the tensor mode perturbation equations given in §III C for the case of pure tension branes. The governing bulk wave equation is separable in Gaussian-normal coordinates, which allows for a Kaluza-Klein mode decomposition of the gravitational wave amplitude  $E$ . Within the spectrum, one can always find a single discrete mode that is normalizable in the bulk. The 4-dimensional mass of this excitation is given by [12, 25]

$$\frac{m_0^2}{H^2} = \begin{cases} \frac{3Hr_c - 1}{(Hr_c)^2}, & \epsilon = +1 \text{ and } Hr_c > 2/3, \\ 0, & \epsilon = -1. \end{cases} \quad (62)$$

In practical terms, the existence of this bound state means that for any choice of initial data, we expect the late time behaviour of the brane amplitude to be well described by a solution of

$$\ddot{E}_b + 3H\dot{E}_b + \left(\frac{k^2}{a^2} + m_0^2\right)E_b = 0, \quad (63)$$

where  $a = a(t) = e^{Ht}$ . It is easy to verify that this implies

$$\lim_{t \rightarrow \infty} E_b(t) \propto \begin{cases} a^{-1/Hr_c}, & \epsilon = +1 \text{ and } Hr_c > 2/3, \\ a^0, & \epsilon = -1. \end{cases} \quad (64)$$

In Fig. 3, we plot a few typical results for the on brane profile of  $E$ . All simulations share the property that they approach scaling solutions at late time:

$$E_b \xrightarrow[t \rightarrow \infty]{} a^{-\gamma}. \quad (65)$$

In all of our simulations for  $\epsilon = -1$ , we find that  $\gamma = 0$ , which is consistent with the analytic expectation that the normal branch spectrum contains a massless bound state. On the other hand, for the self-accelerating brane we would expect

$$\gamma = \frac{1}{Hr_c}, \quad \epsilon = +1. \quad (66)$$

Also in Fig. 3, we plot this theoretical expectation versus our numerical results, and we see excellent agreement. Hence, we have confirmed that our code reproduces analytic results for the gravitational waves in the pure tension DGP model.

## VI. SCALAR PERTURBATIONS IN THE SELF-ACCELERATING UNIVERSE

### A. Cosmological parameters for DGP late-time acceleration

In this section, we concentrate on the  $w = \sigma = 0$  and  $\epsilon = +1$  DGP scenario as a model for the late-time accelerating universe. Examining Table I and Eqns. (19,23,39)



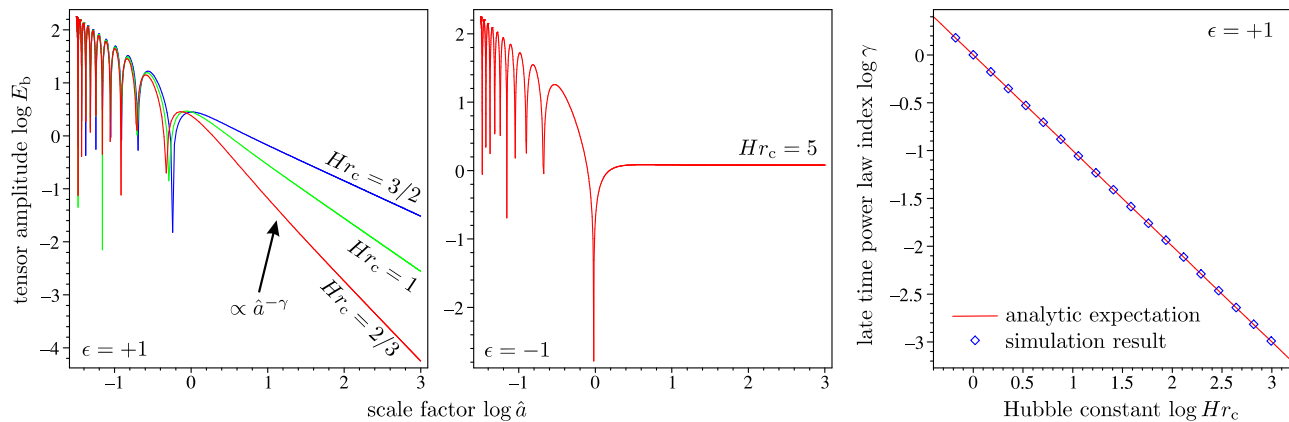


FIG. 3: Numeric solutions for the amplitude of tensor mode perturbations  $E_b$ , on a pure tension brane (left and center) and comparison of the late time power law index derived from analytic and simulation results (right). Note that our late time simulation results for  $\epsilon = -1$  are all very similar to the  $Hr_c = 5$  case shown here, and are all consistent with the analytic  $\gamma = 0$  expectation.

in detail, we see that the entire evolution of scalar perturbations (modulo initial data) in the canonical formalism is governed by a single parameter  $\hat{\rho}_*$ . Recall that we defined  $\hat{\rho}_*$  to be proportional to the matter density when the mode being modeled crosses the Hubble horizon. However, we note that in any model which asymptotes to de Sitter space in the future, any mode that enters the horizon must exit it as well. Indeed, by solving the equation  $\hat{k}/\hat{H}\hat{a} = 1$ , we find that there are always two horizon crossing epochs:

$$\hat{a} = 1 \text{ and } \frac{2\hat{\rho}_*}{3 + \sqrt{9 + 12\hat{\rho}_*}}. \quad (67)$$

If  $\hat{\rho}_* > 6$ , the second solution is always greater than the first; i.e., the perturbation enters the horizon at  $\hat{a} = 1$  and leaves later. However, if  $\hat{\rho}_* = 6$  both solutions coincide and horizon entry and exit occur at the same time. It is easy to confirm that the physical wavelength of the  $\hat{\rho}_* = 6$  mode coincides with the Hubble length at the moment when the brane switches from the decelerating to the accelerating phase; i.e., when  $\ddot{a} = 0$ .

We can go further by incorporating data from cosmological observations. By examining probes of the expansion history [18], it has been found that

$$\Omega_{r_c} = \frac{1}{4H_0^2 r_c^2} = 0.15 \pm 0.02, \quad (68)$$

at 95% confidence.<sup>4</sup> Once the value of  $\Omega_{r_c}$  is fixed, we can use it to find the value of  $a_*$  for any given mode in terms of  $\hat{\rho}_*$ :

$$a_*^3 = \frac{1}{\hat{a}_0^3} = \frac{3(1 - 2\Omega_{r_c}^{1/2})}{4\Omega_{r_c}\hat{\rho}_*}. \quad (69)$$

This in turn allows us to determine the comoving wavenumber from

$$k = \frac{\hat{k}a_*}{r_c} = 2\Omega_{r_c}^{1/2}\hat{k}a_*H_0, \quad H_0^{-1} = 2998 h^{-1} \text{ Mpc}. \quad (70)$$

Hence, we can find  $k$  in terms of  $\hat{\rho}_*$ . In order to facilitate the comparison of our results with observations and the literature, it is more convenient to invert the procedure to obtain  $\hat{\rho}_*$  in terms of  $k$ . However, this only works if  $k$  is above a critical value

$$k_c = 2\Omega_{r_c}^{1/6}(1 - 2\Omega_{r_c}^{1/2})^{1/3}H_0 = 0.0003 h \text{ Mpc}^{-1}. \quad (71)$$

The last equality follows from taking the best fit value for  $\Omega_{r_c}$ , which is what we do from now on. Any modes with  $k < k_c$  have physical wavelengths larger than the Hubble length throughout the cold dark matter and late time acceleration epochs, and therefore are not modeled by our code. Finally, it is sometimes useful to have an explicit expression for the gravitational master variable  $\Omega_b$  in terms of the canonical field  $\psi_b$ . This is:

$$\Omega_b = \frac{a_*}{4H_0^2\Omega_{r_c}}\hat{a}^{3/2}\psi_b = \frac{a_*}{4H_0^2\Omega_{r_c}}\hat{\Omega}_b. \quad (72)$$

## B. Typical waveforms

In Fig. 4, we plot the results of our simulations for several values of  $k$  greater than the critical value  $0.0003 h \text{ Mpc}^{-1}$ . For all plots of scalar perturbations in this paper, we select the bulk field to be zero and the brane field non-zero initially. We have also simulated several different choices of initial data, such as the bulk field being constant along the initial null hypersurface, and have found that the simulation results remain the same as long as the initial time is early enough. This is analogous to what happens in the RS case [11].

<sup>4</sup> Actually, in [18] the constraint  $\Omega_m = 0.23 \pm 0.04$  was given, from which (68) can be easily derived.

From Fig. 4 it can be seen that we recover ordinary 4-dimensional GR at very early times. In particular, for  $a \ll a_*$  and all values of  $k > k_c$  we see that:

- the metric perturbations are conserved and have the opposite sign,  $\Phi \approx -\Psi$ ;
- the density perturbation is proportional to the scale factor,  $\Delta \propto a$ ; and,
- the bulk master variable scales as  $\Omega_b \propto a^4$  on the brane.

In addition, we have checked that the 4-dimensional Poisson equation is satisfied before horizon entry:

$$\frac{k^2}{a^2}\Phi - \frac{1}{2}\kappa_4^2\rho\Delta \approx 0, \quad a \ll a_*. \quad (73)$$

In other words, we have explicitly confirmed that DGP perturbations behave as in GR on superhorizon scales before horizon crossing.

Finally, in Fig. 5 we plot the simulation results for the behaviour of the curvature perturbation  $\zeta$  as given by (37) for a few different large scales. As can clearly be seen,  $\zeta$  is conserved for both early and late times when the physical wavelengths of the modes are much larger than the horizon size. This is to be expected for any metric theory of gravity [23], and hence provides a good consistency check of our code.

### C. The quasi-static approximation and subhorizon behaviour

In [8], a ‘quasi-static’ (QS) approximation was developed to describe the behaviour of DGP perturbations whilst well inside the cosmological horizon and with physical wavelengths much less than the crossover scale:

$$k \gg Ha, \quad a \ll kr_c. \quad (74)$$

These conditions will hold for modes with  $k \gg k_c$  and  $k \gg 2\Omega_{r_c}^{1/2}H_0$  (up to some redshift); or, equivalently, if

$$k \gg 10^{-4} h \text{ Mpc}^{-1}. \quad (75)$$

In this section, we compare the QS approximation to our simulations to determine just how large  $k$  must be for it to be valid.

In the QS approximation, one neglects the time derivatives of  $\Omega$  compared to the spatial gradients. This allows one to solve the bulk wave equation (28), and hence close the system (32) and (33) on the brane. This leads to the following ordinary differential equation for  $\Delta$ :

$$\ddot{\Delta} + 2H\dot{\Delta} = \frac{1}{2}\kappa_4^2 \left(1 + \frac{1}{3\beta}\right), \quad (76)$$

where

$$\beta = 1 - 2\epsilon H r_c \left(1 + \frac{\dot{H}}{3H^2}\right). \quad (77)$$

In addition, the following relations are predicted to hold:

$$\Phi = +\frac{\kappa_4^2\rho a^2}{2k^2} \left(1 - \frac{1}{3\beta}\right) \Delta, \quad (78a)$$

$$\Psi = -\frac{\kappa_4^2\rho a^2}{2k^2} \left(1 + \frac{1}{3\beta}\right) \Delta. \quad (78b)$$

In Fig. 6, we compare simulation results versus the QS approximation for the linear growth factor  $g(a) = \Delta(a)/a$ , and the alternate gravitational potentials  $\Phi_{\pm} = \frac{1}{2}(\Phi \pm \Psi)$ . We see that the simulation results are consistent with the QS approximation for  $k \gtrsim 10^{-2} h \text{ Mpc}^{-1}$ .

We further quantify the performance of the QS approximation in Fig. 7. There, we show the relative error in the QS approximation as a function of the scale. This is defined by

$$\text{rel. error} = \left| \frac{\text{QS prediction} - \text{simulation result}}{\text{simulation result}} \right| \times 100\%. \quad (79)$$

We see that the relative error in the QS prediction for  $\Delta$  is fairly low ( $< 4\%$ ) on all scales. Conversely, the QS values of  $\Phi_{\pm}$  become reliable only for  $k \gtrsim 0.01 h \text{ Mpc}^{-1}$ , with errors of less than  $\sim 5\%$ .

### D. Superhorizon behaviour in the asymptotic future

In this subsection, we attempt to explain/predict the very late time behaviour of our simulations by demonstrating that there exists a bound state of the bulk field in the asymptotic future of the evolution. As we have already seen for the case of tensor perturbations in §V, such bound states tend to dominate the late time behaviour of the model, irrespective of initial data.

In the asymptotic future, the brane geometry approaches that of de Sitter space with  $H = 1/r_c$ . In the de Sitter regime, the bulk wave equation (28) becomes

$$0 = -\frac{\partial^2\Omega}{\partial t^2} + \frac{3}{r_c}\frac{\partial\Omega}{\partial t} + \left(1 + \frac{y}{r_c}\right)^2 \frac{\partial^2\Omega}{\partial y^2} - \frac{2}{r_c}\left(1 + \frac{y}{r_c}\right) \frac{\partial\Omega}{\partial y} - \frac{k^2}{a^2}\Omega, \quad (80)$$

with  $a = e^{t/r_c}$ . This equation is solvable via the separation of variables  $\Omega(t, y) = T_{\lambda}(t)\omega_{\lambda}(y)$ , where

$$0 = \frac{d^2T_{\lambda}}{dt^2} - \frac{3}{r_c}\frac{dT_{\lambda}}{dt} + \left(\frac{k^2}{a^2} - \frac{\lambda}{r_c^2}\right)T_{\lambda}, \quad (81a)$$

$$0 = \frac{d}{dy} \left[ \frac{1}{(y+r_c)^2} \frac{d\omega_{\lambda}}{dy} \right] - \frac{\lambda}{(y+r_c)^4} \omega_{\lambda}. \quad (81b)$$

Here,  $\lambda$  is a dimensionless separation constant. The solution for  $\omega_{\lambda}$  is

$$\omega_{\lambda} = a_+ \left(1 + \frac{y}{r_c}\right)^{\nu_+} + a_- \left(1 + \frac{y}{r_c}\right)^{\nu_-}, \quad (82)$$

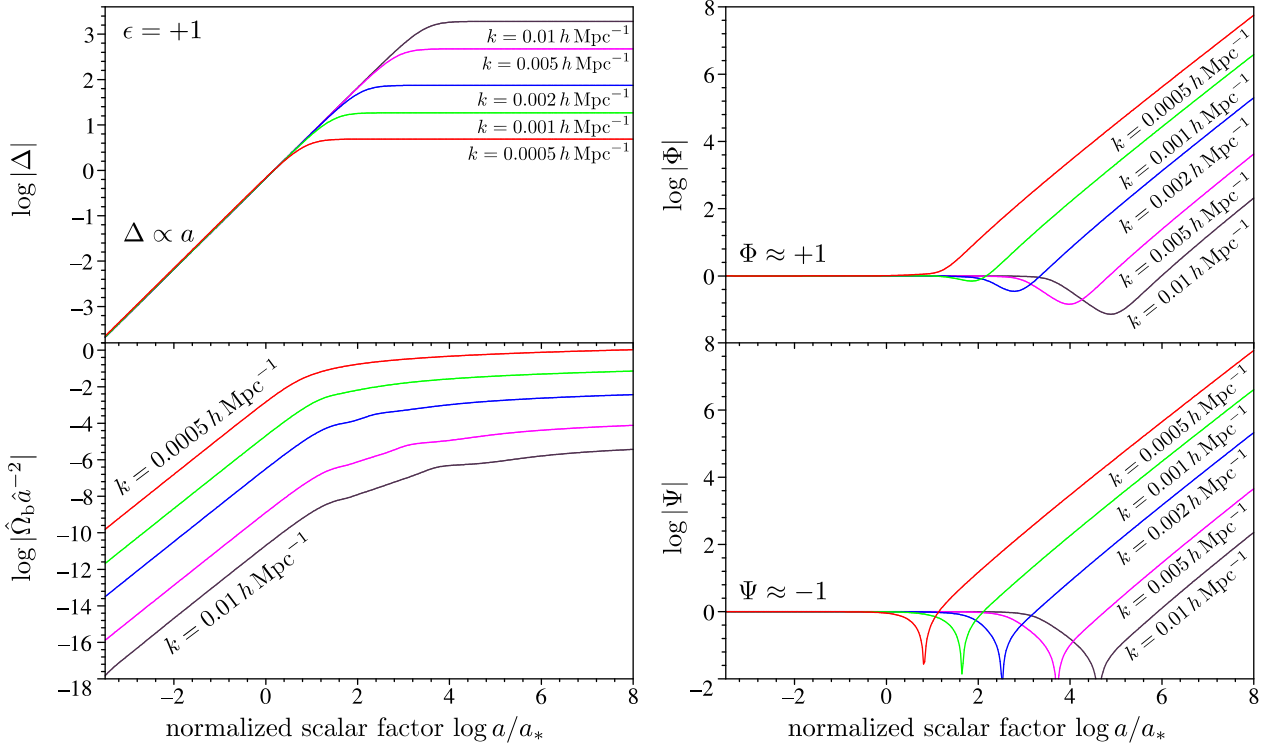


FIG. 4: The results of our simulations on the brane for several choices of  $k$ . We have normalized the value of  $\Phi$  to be unity at early times. Also note that the lower left panel shows the dimensionless bulk master variable  $\hat{\Omega}_b$ , as defined in Eq. (40), divided by  $\hat{a}^2$ . All simulations are performed with  $\hat{\rho}_* > 6$ , which means that all modes *enter* the horizon at  $\hat{a} = 1$ , or when  $a = a_*$ .

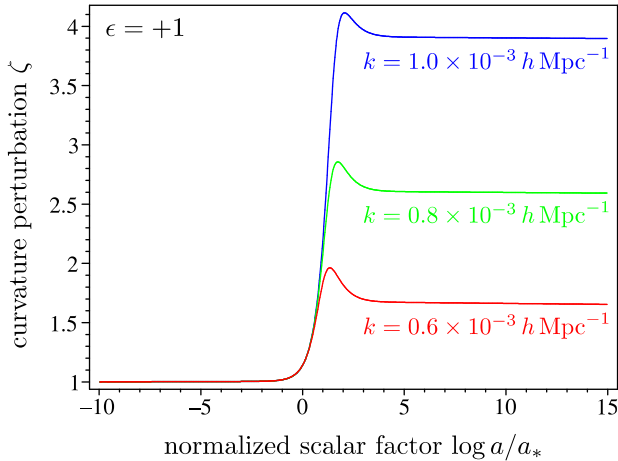


FIG. 5: Behaviour of the  $\zeta$  curvature perturbation on large scales for the self-accelerating branch (we have normalized  $\zeta = 1$  at early times). Note that the curvature perturbation is conserved when the modes are superhorizon; i.e., at both early and late times. This is to be expected for any conservative theory of gravity, such as the DGP model.

where  $\nu_{\pm} = \frac{3}{2} \left( 1 \pm \sqrt{1 + \frac{4}{9}\lambda} \right)$ . Assuming that  $\lambda$  is real, we need to set  $a_+ = 0$  to ensure that  $\omega_{\lambda}$  is normalisable

under the Sturm-Louisville inner product; i.e., that

$$(\omega_{\lambda}, \omega_{\lambda}) = \int_0^{\infty} dy \frac{\omega_{\lambda}^2(y)}{(y + r_c)^4}, \quad (83)$$

is finite, which means we have a true bound state.

Now, if we put  $H = 1/r_c$  in the boundary condition (32) we obtain

$$(\partial_y \Omega)_b = -r_c \left[ \ddot{\Omega}_b - \frac{3}{r_c} \dot{\Omega}_b + \left( \frac{k^2}{a^2} + \frac{1}{r_c^2} \right) \Omega_b - \frac{2\kappa_4^2 \rho a^3}{k^2} \Delta \right]. \quad (84)$$

Let us now assume that for very late times ( $kr_c \ll a$ ) the following conditions hold:

$$\left| \frac{\kappa_4^2 \rho a^3}{k^2} \Delta \right| \ll \min \left( |\ddot{\Omega}_b|, r_c^{-1} |\dot{\Omega}_b|, r_c^{-2} |\Omega_b| \right); \quad (85)$$

i.e., the  $\Delta$  term is negligible on the righthand side of (84). Under these assumptions, which we still need to justify, (80) and (84) form a closed system for  $\Omega$ . Putting our mode solution  $\Omega(t, y) = T_{\lambda}(t)\omega_{\lambda}(y)$  into the boundary condition with  $c_+ = 0$  and neglecting  $\Delta$ , we obtain

$$\lambda = -2. \quad (86)$$

Putting  $\lambda = -2$  into the temporal equation (81a) and solving for  $T_{\lambda}$ , we find that

$$T_{\lambda}(t) \xrightarrow[t \rightarrow \infty]{} b_1 a^2(t) + b_2 a(t), \quad (87)$$

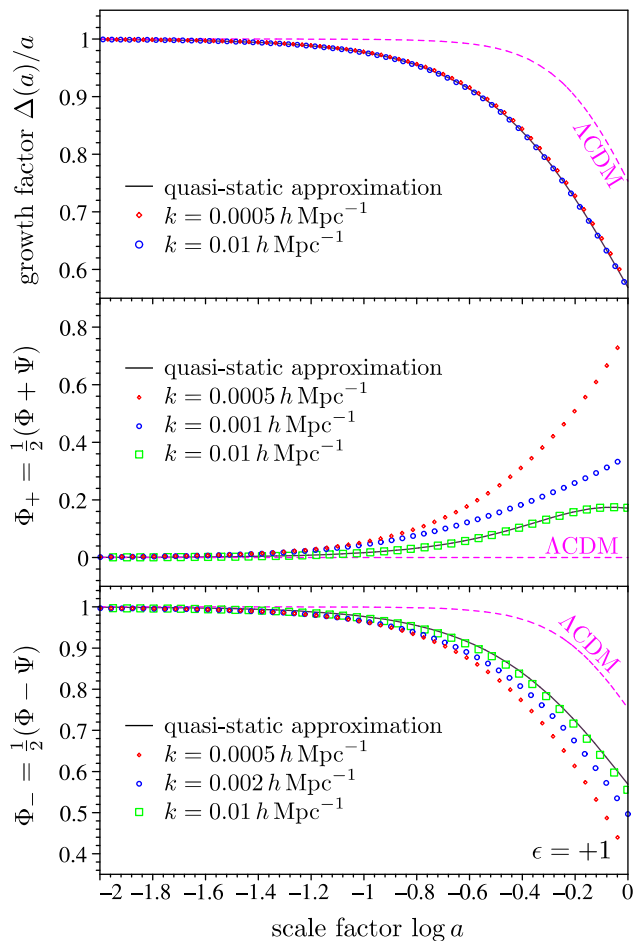


FIG. 6: Linear growth factor and alternate gravitational potentials  $\Phi_{\pm}$  from simulations and the QS approximation in the self-accelerating branch. In the top panel, we normalize  $g(a)$  to unity at early times, in the lower two panels we normalize  $\Phi_{-}$  to unity as  $a \rightarrow 0$ . For comparison, we also show the relevant results for the concordance  $\Lambda$ CDM model with  $\Omega_m = 0.26$  and  $\Omega_{\Lambda} = 0.74$ .

where  $b_1$  and  $b_2$  are constants. Of course, the  $b_1$  solution will eventually dominate, which leads to the following asymptotic bound state:

$$\Omega(t, y) \xrightarrow{t} \Omega_0 \left(1 + \frac{y}{r_c}\right) a^2(t), \quad (88)$$

where  $\Omega_0$  is a constant. However, before we assume that the late time behaviour of the system is indeed described by this bound state, we must verify that the assumptions (85) under which it was derived are valid. To do so, we note that when  $H = 1/r_c$ , the  $\Delta$  equation of motion (33) reduces to

$$\ddot{\Delta} + \frac{2}{r_c} \dot{\Delta} - \kappa_4^2 \rho \Delta = -\frac{k^4}{3a^5} \Omega_b. \quad (89)$$

Making use of (88), this equation can be solved exactly. However, the full solution is complicated and not really

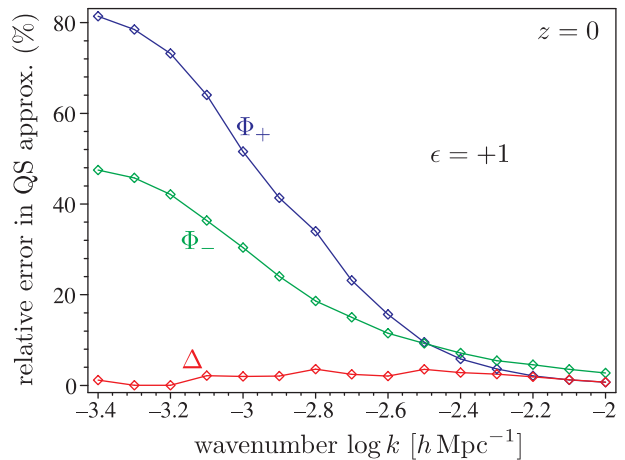


FIG. 7: The relative error in the QS approximation, as defined in Eq. (79), for various quantities evaluated in the present epoch and assuming the self-accelerating branch. For  $k \gtrsim 0.01 h \text{ Mpc}^{-1}$  the errors are less than 5%.

relevant, so we just quote the late time behaviour

$$\Delta(t) \xrightarrow{t} \Delta_0, \quad (90)$$

where  $\Delta_0$  is a constant. With the solutions (88) and (90), we see that the assumptions (85) are indeed satisfied at sufficiently late time. Hence we have succeeded in finding an asymptotic bound state that is expected to dominate the system's behaviour at late time. Finally, note that we can use these asymptotic solutions for  $\Omega$  and  $\Delta$  with (34) to obtain

$$\Phi \xrightarrow{t} \frac{\Omega_0 a(t)}{2r_c^2}, \quad \Psi \xrightarrow{t} \frac{\Omega_0 a(t)}{2r_c^2}; \quad (91)$$

i.e.,  $\Phi \approx \Psi$  at late time. We have verified that the asymptotic solutions (88,90,91) are realized in our simulations at late times.

Before moving on, we would like to remark on the apparent instability of the self-accelerating DGP model as indicated by the divergence of  $\Omega$ ,  $\Phi$  and  $\Psi$  in the asymptotic future. This unstable mode corresponds to the radion, which is a physical degree of freedom in the self-accelerating branch despite the fact that we have only one brane [12]. It is well known that in this case the radion has a negative mass squared  $m^2 = -4H^2$  and thus it is unstable [26]. However, as was shown in Ref. [27], this is not a true gravitational instability on the brane as it is possible to find a gauge in which all metric perturbations remain finite.

## VII. SCALAR PERTURBATIONS IN THE DGP NORMAL BRANCH

### A. Cosmological parameters for $\Lambda$ DGP

We now turn our attention to the behaviour of density perturbations in the normal branch of the DGP model. Unlike the  $\epsilon = +1$  case, this branch does not naturally have a late time accelerating phase. So in order to be made consistent with observations, we must allow for the brane to have a nonzero tension that acts as an effective 4-dimensional cosmological constant (we call this the  $\Lambda$ DGP model). Assuming that the matter sector is CDM-dominated, the Friedmann equation for this scenario follows from the general form (15) with  $\epsilon = -1$  and  $w = 0$ . The background dynamics has been compared to observations of  $H(z)$  in [18], who finds the following parameter values:

$$\Omega_m = \frac{\kappa_4^2 \rho_0}{3H_0^2} = 0.23 \pm 0.04, \quad \Omega_{r_c} = \frac{1}{4H_0^2 r_c^2} \leq 0.05, \quad (92)$$

at 95% confidence. Here,  $\rho_0$  is the present day CDM density. Note that the observationally preferred value of  $\Omega_{r_c}$  is zero. Since the DGP model goes over to GR in this limit, this implies that  $\Lambda$ CDM gives a better fit to the data than  $\Lambda$ DGP. In what follows, we will always assume the best fit value of 0.23 for  $\Omega_m$  and treat  $\Omega_{r_c}$  as an adjustable parameter that must be smaller than 0.05 to yield a realistic model.

Once  $\Omega_m$  and  $\Omega_{r_c}$  have been selected, it is straightforward to obtain the value of the dimensionless brane tension:

$$\hat{\sigma} = \kappa_4^2 r_c^2 \sigma = \frac{3(1 - \Omega_m + 2\Omega_{r_c}^{1/2})}{4\Omega_{r_c}}, \quad (93)$$

which can be re-written in terms of a new density parameter  $\Omega_\sigma$ :

$$\Omega_\sigma = \frac{\kappa_4^2 \sigma}{3H_0^2} = 1 - \Omega_m + 2\Omega_{r_c}^{1/2}. \quad (94)$$

One can also find  $a_*$  in terms of the observational parameters and  $\hat{\rho}_*$ :

$$a_*^3 = \frac{1}{\hat{a}_0^3} = \frac{3\Omega_m}{4\Omega_{r_c} \hat{\rho}_*}. \quad (95)$$

As before, these two formulae can be used in (70) to determine  $k$  as an explicit function of  $\hat{\rho}_*$ , or  $\hat{\rho}_*$  as an implicit function of  $k$ . Following the latter approach means that when we select  $k$  along with  $\Omega_m$  and  $\Omega_{r_c}$ , the evolution of perturbations is completely specified up to the choice of initial data.

### B. Simulation results and comparison to the QS approximation

In Fig. 8, we compare the results of our simulations to the QS approximation and  $\Lambda$ CDM in the case  $\Omega_{r_c} = 0.05$ .

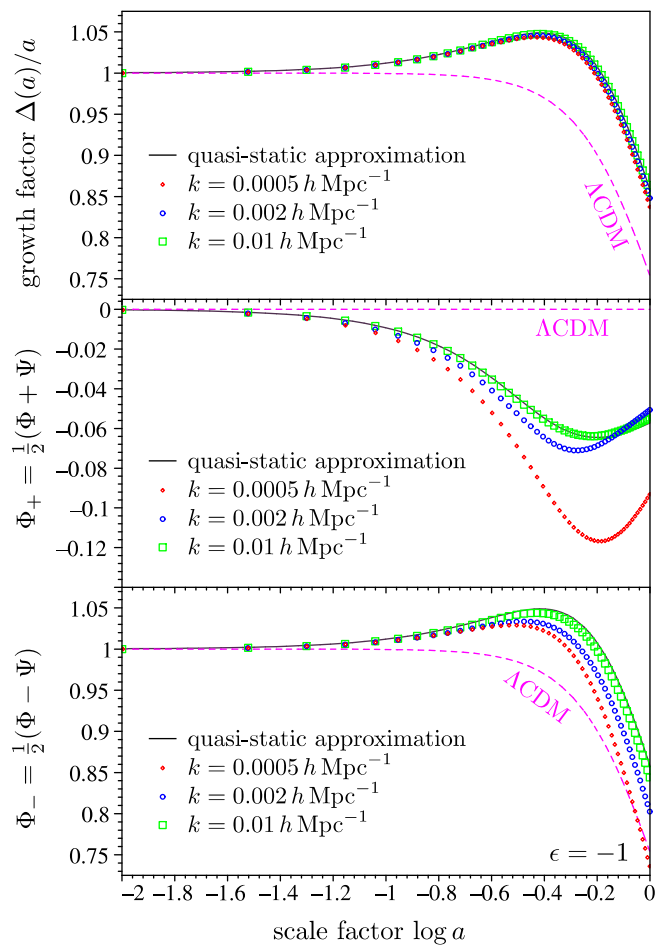


FIG. 8: Linear growth factor and alternate gravitational potentials  $\Phi_{\pm}$  from simulations and the QS approximation in the normal branch with  $\Omega_{r_c} = 0.05$  and  $\Omega_m = 0.23$ . As in Fig. 6, we normalize  $g(a)$  and  $\Phi_{\pm}$  to unity at early times. For comparison, we also show the relevant results for the concordance  $\Lambda$ CDM model with  $\Omega_m = 0.26$  and  $\Omega_{\Lambda} = 0.74$ .

As in §VIB, we find that the simulation results are fairly insensitive to initial conditions provided that the initial data surface is set far enough into the past; here, all plots have been generated assuming  $\Omega = 0$  initially. In contrast to the self-accelerating case, we find that the linear growth factor and  $\Phi_{-}$  potential are generally larger than in the  $\Lambda$ CDM case. The general trend is for  $\Phi_{-}$  to become larger on small scales. We also notice that the QS approximation seems to provide a very good match to the simulation results for  $\Delta$  on all scales.

In Fig. 9, we show the effect of changing the  $\Omega_{r_c}$  parameter on the simulation results for  $\Phi_{-}$ . For any given scale, we see that the  $\Omega_{r_c} \rightarrow 0$  limit approaches the  $\Lambda$ CDM prediction. Also, we note that the simulation results are closer to the  $\Lambda$ CDM case for smaller values of  $k$ ; i.e., the most pronounced deviations from GR are observed on the smallest scales simulated.

Finally, in Fig. 10 we quantify the error in the QS prediction for the value of various quantities at  $z = 0$

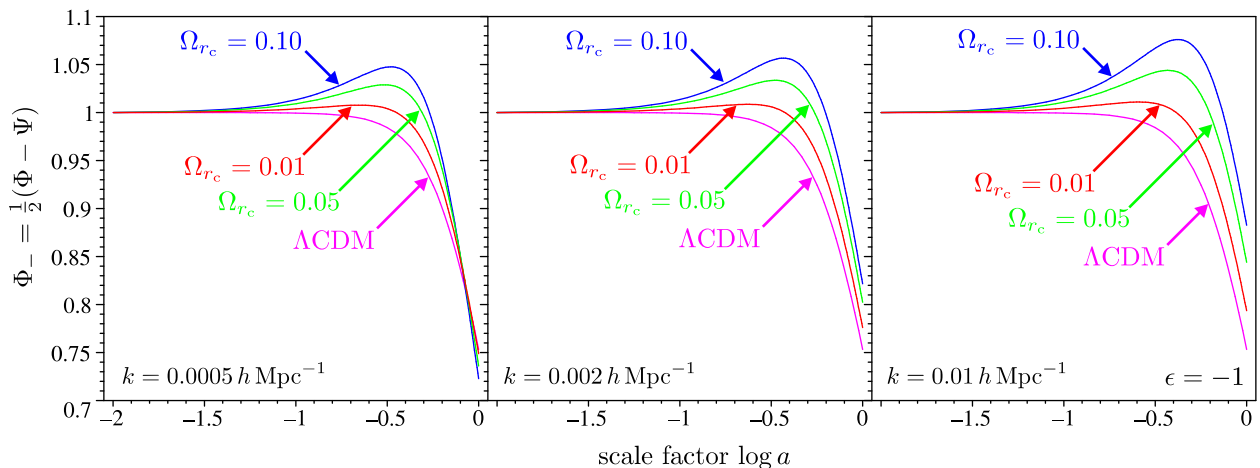


FIG. 9: The ‘ISW potential’  $\Phi_-$  as a function of the scale factor for various scales and choices of  $\Omega_{r_c}$  for the normal branch. In all cases we have taken  $\Omega_m = 0.23$ . The  $\Lambda$ CDM curves are included for purposes of comparison.

as a function of the scale. As in the self-accelerating case, we see that the QS approximation provides reasonably accurate results (with errors  $\lesssim 5\%$ ) on scales  $k \gtrsim 0.01 h \text{ Mpc}^{-1}$ .

### C. Superhorizon behaviour in the asymptotic future

In the asymptotic future, the brane geometry approaches that of de Sitter spacetime with  $H$  determined by  $\sigma \neq 0$ . Unlike in the self-accelerating branch, there appears a horizon at  $y = 1/H$ . An analysis similar to the one presented in §VID for the self-accelerating branch shows that there is no solution with a real  $\lambda$  [28]. Therefore, there is no bound state solution in the asymptotic de Sitter spacetime and  $\Omega$  is a superposition of massive Kaluza-Klein modes that oscillate in time. It is worth noting that the dynamical scaling *ansatz* implicitly assumes the existence of a  $\Omega$  bound state, and will hence fail in the asymptotic de Sitter future of the DGP normal branch.

## VIII. CONCLUSIONS

In this paper, we have presented numeric solutions for cosmological perturbations in the DGP braneworld model both in the self-accelerating and the normal branches. We extended the algorithm developed for the Randall-Sundrum (RS) model to handle the nonlocal boundary conditions characteristic of the DGP model. The numerical code was tested for tensor perturbations and the agreement with the analytic solutions was found to be excellent.

We confirmed that on small scales  $k > 0.01 h \text{ Mpc}^{-1}$ , the quasi-static (QS) approximation reliably predicts the evolution of perturbations with relative errors less than

around 5% at  $z = 0$ . Our results are quite insensitive to the initial conditions as long as we start our simulations early enough. On larger scales, the potential  $\Phi_-$ , which determines the integrated Sachs-Wolfe (ISW) effect, shows more suppression than the QS prediction. We find that our numerical solutions agree well with the dynamical scaling (DS) solution both in the self-accelerating and normal branches, except in the asymptotic de Sitter phase of the normal branch where the dynamical scaling solution fails to exist [29].

Our numeric solutions provide the basis for studying observational signatures of the model, especially in the normal branch where the influence of the extra dimension on the evolution of large scale structure has not yet been explored.

### Acknowledgments

We would like to thank Roy Maartens and Yong-Seon Song for many useful conversations. AC is supported by FCT (Portugal) PhD fellowship SFRH/BD/19853/2004. KK is supported by STFC (UK). SSS is supported by STFC (UK) and NSERC (Canada). FPS is supported by FCT (Portugal) PhD fellowship SFRH/BD/27249/2006.

## APPENDIX A: BOUNDARY CONDITION AND $\Delta$ EQUATION OF MOTION FOR SCALAR PERTURBATIONS

To derive the boundary condition satisfied by the bulk master variable  $\Omega$  and the second order equation of motion for the density perturbation  $\Delta$  for scalar perturbations, we begin with the linearized version of the effective Einstein equations (7):

$$\delta G_{\mu\nu}^{(4)} = (2\kappa_4^2 r_c)^2 \delta \Pi_{\mu\nu} - \delta \mathcal{E}_{\mu\nu}. \quad (\text{A1})$$

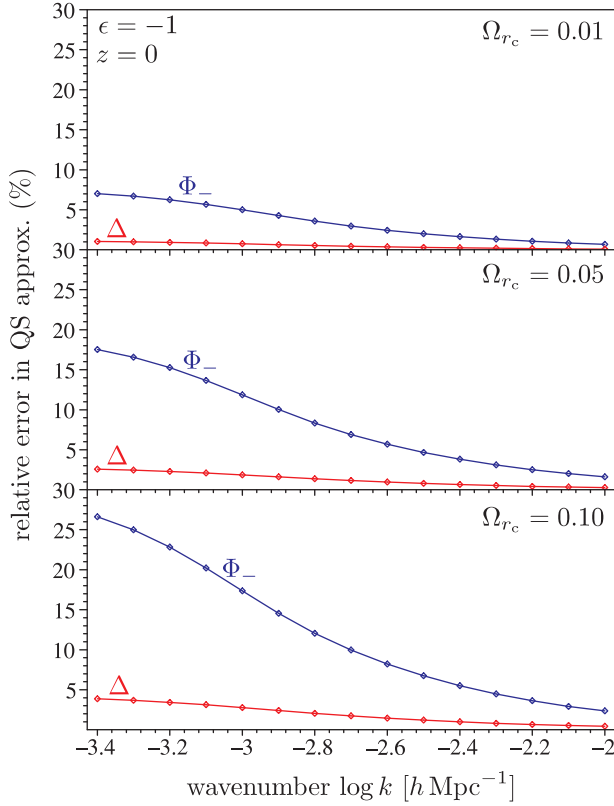


FIG. 10: The relative error in the QS approximation, as defined in Eq. (79), for various quantities evaluated in the present epoch and assuming the normal branch. For  $k \gtrsim 0.01 h \text{Mpc}^{-1}$  the errors are less than 5%. Also notice how the QS approximation is generally more accurate for smaller  $\Omega_{rc}$ .

In this expression,  $\delta G_{\mu\nu}^{(4)}$  and  $\delta \Pi_{\mu\nu}$  can be obtained by using the perturbed brane metric (29) and perturbed stress energy tensor (30). We can parameterize the perturbations of the bulk Weyl “fluid”  $\mathcal{E}_{\mu\nu}$  as follows:

$$\delta \mathcal{E}_{\nu}^{\mu} = -\kappa_4^2 \begin{pmatrix} -\delta \rho_{\mathcal{E}} & a \delta q_{\mathcal{E},i} \\ a^{-1} \delta q_{\mathcal{E},i} & \frac{1}{3} \delta \rho_{\mathcal{E}} \delta^i_j + \delta \pi_{\mathcal{E},j}^i \end{pmatrix}. \quad (\text{A2})$$

Here,  $\delta \pi_{ij}^{\mathcal{E}} = \delta \pi_{,ij}^{\mathcal{E}} - \frac{1}{3} \delta \pi_{,k}^{\mathcal{E},k} \delta_{ij}$ , a comma denotes partial differentiation and indices are raised and lowered with the flat 3-metric. Using this in the  $(0, i)$  component of the perturbed effective Einstein equations (A1), we obtain the following equation:

$$H\Psi - \dot{\Phi} = \frac{\kappa_4^2}{2} \left( \frac{2Hr_c\epsilon}{2Hr_c\epsilon - 1} \right) \left( \frac{\rho V}{k} + \frac{\delta q_{\mathcal{E}}}{2Hr_c\epsilon} \right), \quad (\text{A3})$$

where we have made use of the fact that the background brane matter distribution is CDM plus a possible effective cosmological constant induced by the brane tension. Combining this with the  $(0, 0)$  component of (A1) yields the Poisson equation:

$$\frac{k^2}{a^2} \Phi = \frac{\kappa_4^2}{2} \left( \frac{2\epsilon Hr_c}{2\epsilon Hr_c - 1} \right) \left( \rho \Delta - \frac{\delta \rho_{\mathcal{E}} - 3H\delta q_{\mathcal{E}}}{2\epsilon Hr_c} \right). \quad (\text{A4})$$

In these formulae, the gauge invariant density perturbation  $\Delta$  is defined in (31), while the invariant velocity perturbation is given by  $V = -k \delta q / \rho$  in the longitudinal gauge.

Additional relations can be obtained by noting that

$$\delta(\nabla^{\alpha} T_{\alpha\beta}) = 0. \quad (\text{A5})$$

The spatial and temporal components of this yield that

$$\dot{V} + HV = \frac{k}{a} \Psi, \quad (\text{A6a})$$

$$\dot{\Delta} = -\frac{k}{a} \left( 1 - \frac{3a^2}{k^2} \dot{H} \right) V - 3(\dot{\Phi} - H\Psi), \quad (\text{A6b})$$

respectively. Combining (A3) with (A6) yields a second order differential equation for  $\Delta$ :

$$\ddot{\Delta} + 2H\dot{\Delta} = -\frac{k^2}{a^2} \Psi + \frac{3}{2} \dot{F} + 3HF, \quad (\text{A7})$$

with

$$F = \frac{\kappa_4^2 \delta q_{\mathcal{E}}}{2Hr_c\epsilon - 1}. \quad (\text{A8})$$

Now, one important feature that distinguishes braneworld cosmological fluctuations from the GR case is that in addition to perturbations of the geometry and the matter, we must also consider perturbations of the brane’s position. That is, in the Gaussian normal coordinates system the brane is located at  $y = 0$  before perturbation and at  $y = \xi$  after perturbation, where  $\xi$  is the scalar brane bending degree of freedom. It is useful to parameterize the perturbed geometry of the  $y = 0$  hypersurface (i.e., the brane’s unperturbed position) by

$$ds_{y=0}^2 = -(1 + 2\mathcal{A})dt^2 + a^2(1 + 2\mathcal{R})\delta_{ij}dx^i dx^j. \quad (\text{A9})$$

The metric potentials at the unperturbed brane position ( $\mathcal{A}, \mathcal{R}$ ) are then related to the metric potentials at the perturbed position ( $\Psi, \Phi$ ) by

$$\Psi = \mathcal{A} - \epsilon \left( \frac{\dot{H}}{H} + H \right) \xi, \quad \Phi = \mathcal{R} - \epsilon H \xi. \quad (\text{A10})$$

Deffayet [22] has shown that the brane bending scalar is simply given by

$$\xi = -r_c(\Phi + \Psi). \quad (\text{A11})$$

In addition, he demonstrated that it is possible to express  $\mathcal{A}$  and  $\mathcal{R}$  in terms of the bulk master variable  $\Omega$ :

$$\begin{aligned} \mathcal{A} &= \frac{1}{6a} \left[ 3\epsilon \left( \frac{\dot{H}}{H} - H \right) (\partial_y \Omega)_b + \frac{2k^2}{a^2} \Omega_b - 3\ddot{\Omega}_b + 6H\dot{\Omega}_b \right], \\ \mathcal{R} &= \frac{1}{6a} \left[ 3\epsilon H (\partial_y \Omega)_b + \frac{k^2}{a^2} \Omega_b - 3H\dot{\Omega}_b \right]. \end{aligned} \quad (\text{A12})$$

It can also be shown [22] that the Weyl fluid perturbations are also directly given by  $\Omega$ :

$$\kappa_4^2 \delta \rho_{\mathcal{E}} = \frac{k^4 \Omega}{3a^5}, \quad \kappa_4^2 \delta q_{\mathcal{E}} = -\frac{k^2}{3a^3} (H\Omega - \dot{\Omega}). \quad (\text{A13})$$

Now, these formulae in conjunction with the wave equation (28) can be used to re-write the Poisson equation (A4) as:

$$2r_c \kappa_4^2 \rho \Delta = 4r_c \frac{k^2}{a^2} \Phi + \frac{2k^2}{a^2} \xi - \frac{k^2}{a^3} [(\partial_y \Omega)_b - \epsilon H \Omega_b]. \quad (\text{A14})$$

Then, one can use (A10)–(A12) in this equation to obtain the boundary condition (32). One can then use (32) with (A10)–(A12) to get  $\Phi$  and  $\Psi$  in terms of  $\Omega_b$  and  $\Delta$ ; i.e., Eqs. (34). Finally, substituting (34) and (A13) into (A7) gives the final form of the  $\Delta$  equation of motion (33).

- 
- [1] G. R. Dvali, G. Gabadadze, and M. Porrati, *Phys. Lett.* **B484**, 112 (2000), hep-th/0002190.
- [2] G. R. Dvali, G. Gabadadze, and M. Porrati, *Phys. Lett.* **B485**, 208 (2000), hep-th/0005016.
- [3] C. Deffayet, *Phys. Lett.* **B502**, 199 (2001), hep-th/0010186.
- [4] M. Fairbairn and A. Goobar, *Phys. Lett.* **B642**, 432 (2006), astro-ph/0511029.
- [5] R. Maartens and E. Majerotto, *Phys. Rev.* **D74**, 023004 (2006), astro-ph/0603353.
- [6] Y.-S. Song, I. Sawicki, and W. Hu, *Phys. Rev.* **D75**, 064003 (2007), astro-ph/0606286.
- [7] K. Koyama (2007), arXiv:0706.1557 [astro-ph].
- [8] K. Koyama and R. Maartens, *JCAP* **0601**, 016 (2006), astro-ph/0511634.
- [9] I. Sawicki, Y.-S. Song, and W. Hu, *Phys. Rev.* **D75**, 064002 (2007), astro-ph/0606285.
- [10] A. Cardoso, K. Koyama, A. Mennim, S. S. Seahra, and D. Wands, *Phys. Rev.* **D75**, 084002 (2007), hep-th/0612202.
- [11] A. Cardoso, T. Hiramatsu, K. Koyama, and S. S. Seahra (2007), arXiv:0705.1685 [astro-ph].
- [12] K. Koyama, *Phys. Rev.* **D72**, 123511 (2005), hep-th/0503191.
- [13] D. Gorbunov, K. Koyama, and S. Sibiryakov, *Phys. Rev.* **D73**, 044016 (2006), hep-th/0512097.
- [14] K. Koyama (2007), arXiv:0709.2399 [hep-th].
- [15] V. Sahni and Y. Shtanov, *JCAP* **0311**, 014 (2003), astro-ph/0202346.
- [16] A. Lue and G. D. Starkman, *Phys. Rev.* **D70**, 101501 (2004), astro-ph/0408246.
- [17] R. Lazkoz, R. Maartens, and E. Majerotto, *Phys. Rev.* **D74**, 083510 (2006), astro-ph/0605701.
- [18] R. Lazkoz and E. Majerotto (2007), arXiv:0704.2606 [astro-ph].
- [19] C. Charmousis, R. Gregory, N. Kaloper, and A. Padilla, *JHEP* **10**, 066 (2006), hep-th/0604086.
- [20] Y.-S. Song (2007), arXiv:0711.2513 [astro-ph].
- [21] S. Mukohyama, *Phys. Rev.* **D62**, 084015 (2000), hep-th/0004067.
- [22] C. Deffayet, *Phys. Rev.* **D66**, 103504 (2002), hep-th/0205084.
- [23] D. Wands, K. A. Malik, D. H. Lyth, and A. R. Liddle, *Phys. Rev.* **D62**, 043527 (2000), astro-ph/0003278.
- [24] C. Deffayet, *Phys. Rev.* **D71**, 023520 (2005), hep-th/0409302.
- [25] K. Koyama and K. Koyama, *Phys. Rev.* **D72**, 043511 (2005), hep-th/0501232.
- [26] U. Gen and M. Sasaki, *Prog. Theor. Phys.* **105**, 591 (2001), gr-qc/0011078.
- [27] U. Gen and M. Sasaki, *Prog. Theor. Phys.* **108**, 471 (2002), gr-qc/0201031.
- [28] K. Koyama and S. Mizuno, *JCAP* **0607**, 013 (2006), gr-qc/0606056.
- [29] Y.-S. Song, private communication (2007).